Effect of Propeller Installation on Performance Indicators of Regional Turboprop Aircraft

Schouten, Tom; Hoogreef, Maurice; Vos, Roelof

DOI
10.2514/6.2019-1306

Publication date
2019

Document Version
Final published version

Published in
AIAA Scitech 2019 Forum

AIAA SciTech Forum
7-11 January 2019, San Diego, California
AIAA Scitech 2019 Forum

10.2514/6.2019-1306

Effect of Propeller Installation on Performance Indicators of Regional Turboprop Aircraft

Thomas J. E. Schouten*, Maurice F. M. Hoogreef† and Roelof Vos‡
Delft University of Technology, Delft, 2600AA, The Netherlands

Four regional turboprop aircraft of different configuration are assessed on their key performance indicators by using an automated conceptual design method. The configurations include two wing-mounted propeller installations (high-wing and low-wing) as well as a fuselage-mounted configuration and a tail-mounted configuration. The effect of the propeller and associated slipstream is included in the sizing of the horizontal tail plane of these aircraft. The results from the automated design method are compared to benchmarks from open literature showing a deviation in maximum take-off mass of around 10%. The four different aircraft configurations were applied to aircraft designs for a payload of 130 passengers and a harmonic range of 1500nm (2960km). Results from the configuration study show that the aircraft with propellers mounted on the tail or on the fuselage have about a 5% higher maximum take-off mass than the low-wing, wing-mounted configuration due to the absence of wing bending moment relief and an increase in trim drag resulting from a larger center-of-gravity excursion. The application of natural laminar flow on the clean wing as well as operational bounds on the center-of-gravity excursion were also investigated but did not show an improvement in aircraft performance indicators compared to the low-wing, wing-mounted designs.

Nomenclature

Latin symbols

A	=	aspect ratio (∼)
B_P	=	number of blades
b	=	wing span (m)
$\bar{c}$	=	mean aerodynamic chord (m)
C_D	=	drag coefficient (∼)
C_L	=	lift coefficient (∼)
C_m	=	pitching moment coefficient (∼)
C_T	=	thrust coefficient (∼)
d	=	diameter (m)
h	=	height (m)
L	=	lift force (N)
l	=	length (m)
M	=	pitching moment (N) or Mach number (∼)
N	=	normal force (N)
P	=	max. continuous propeller power (W)
q	=	dynamic pressure (kg/ms^2)
T	=	propeller thrust (N)
V	=	velocity (m/s)
W	=	weight force (N)

Greek Symbols

α	=	angle of attack (°)
Δ	=	symbol denoting change
δ	=	flap deflection angle (°)
ϵ	=	downwash angle (°)
$\dot{\theta}$	=	rate of rotation (°/s^2)
ρ	=	air density (kg/m^3)

Subscripts

0	=	zero-lift
1	=	take-off configuration
ac	=	aerodynamic center
a-h	=	aircraft minus tail
cg	=	center of gravity
f	=	fuselage
h	=	horizontal tail
mlg	=	main landing gear
n	=	nacelle
p	=	propeller
R	=	rotation
S	=	stall
w	=	main wing

*MSc. Student, Faculty of Aerospace Engineering, Delft University of Technology, P.O. Box 5058, 2600 GB Delft, The Netherlands
†Postdoctoral Research Associate, Faculty of Aerospace Engineering, Delft University of Technology, P.O. Box 5058, 2600 GB Delft, The Netherlands, AIAA Member
‡Assistant Professor, Faculty of Aerospace Engineering, Delft University of Technology, P.O. Box 5058, 2600 GB Delft, The Netherlands, Associate Fellow AIAA

Abbreviations

CG	=	center of gravity
BSFC	=	brake-specific fuel consumption
HLD	=	high lift devices
HTP	=	horizontal tail plane
MFM	=	mission fuel mass
MTOM	=	maximum take-off mass
NLF	=	natural laminar flow
OEM	=	operating empty mass
RTP	=	regional turboprop
SFC	=	specific fuel consumption
SM	=	static margin

I. Introduction

Air travel is expected to double over the next 20 years, where three-quarters of the market requires short to medium range regional aircraft to fulfill passenger demand*. New aircraft in this market should perform the envisioned mission at a reduced fuel burn as compared to existing designs, stemming from more stringent aircraft emission regulation together with the desire of airliners to reduce costs. As such, these aircraft could be powered by turbopropeller engines, which are shown to be more fuel-efficient than regional jets on short-to-medium haul missions according to historical data analyzed by Babikian et al.[1]. In this paper, the conceptual design of a next-generation twin-engined regional turboprop (RTP) is presented, which is to carry 130 passengers over a harmonic range of 2960km, similar to the Airbus A220-100 and Embraer E195E2 in terms of passenger capacity but over a significantly shorter range. †

To enhance the cabin comfort and reduce noise from the propellers, the installation of the propeller on the aircraft is of paramount importance. The typical high-wing configuration with engines mounted below the wing places the noise source right next to the cabin. Therefore, this study also investigates alternative configurations with engines placed on pylons on the aft fuselage as well as engines integrated in the horizontal tail plane (see Figure 1). Nicolosi et al. claim that a regional turboprop of the latter configuration can reduce direct operating cost and fuel burn per passenger-kilometer compared to the A220-100[2]. Also Douglas Aircraft Company investigated in the early 1980's a modification of a DC-9 (155-165 pax) with aft-mounted propellers to further increase fuel efficiency showing 25% fuel savings for a 2200km mission compared to the turbofan-powered baseline design. Installation on the horizontal tailplane was found to be most favorable in terms of fuel savings, although it was also concluded that further windtunnel tests and flight tests were required to demonstrate these savings along with adequate handling qualities [3]. However, Vos and Hoogreef showed for a 68-passenger regional aircraft that the propeller installation on the horizontal tail plane causes the center-of-gravity (CG) of the empty aircraft to shift quite far aft, resulting in a large CG excursion during loading and a consequent trim drag penalty leading to a 12% increase in fuel burn over a 1500 km harmonic range [4].

The installation of propellers results in strong airframe-propulsion interaction. This interaction has been studied for wing-mounted propeller installation for example in Veldhuis [5] and the effect on stability and control has been studied by, amongst others, Obert[6]. More recently, Bouquet and Vos showed that slipstream effects need to be incorporated in the conceptual design phase to ensure a sufficiently large tail plane to provide trim capability and static stability over the full center-of-gravity range[7]. For tail-mounted propellers, Van Arnhem et al. performed an experimental and numerical study into the aerodynamic interaction of tip-mounted propellers on a horizontal tail plane, showing a 20% change in the lift-curve slope and elevator effectiveness at an advance ratio of 0.7 attributed to the slipstream effect and, to a lesser degree, the normal force of the propeller [8].

The goal of this paper is to demonstrate how key performance indicators, such as fuel-burn and maximum take-off weight, for a 130-passenger regional turboprop aircraft are affected by the positioning of the propulsion system. To demonstrate this, an in-house developed aircraft design tool, known as the *Aircraft Initiator*, is employed. The Initiator is a multidisciplinary design and analysis system that iteratively sizes transport category aircraft based on a set of top-level requirements [9]. The Initiator has been previously used to assess the impact of new aircraft configurations [10] as well as aircraft technologies [11]. As shown in Ref. [7], the Initiator includes a model for the propeller slipstream and propeller normal force such that these effects are included in the synthesis of the proposed configurations.

The paper is structured as follows. The methods used to perform the investigation are presented in Section II. Next, Section III verifies that the models that are used for tail sizing are adequate and that the resulting designs match closely to existing aircraft and previously performed studies. Section IV shows the performance study for the large turboprop aircraft considering four different configurations: a high-wing aircraft with wing-mounted propellers, a low-wing aircraft with wing-mounted propellers, a low-wing aircraft with fuselage-mounted propellers, and a low-wing aircraft

*Boeing Commercial Airplanes, *"Current Market Outlook 2015-2034,"* 2015. URL `http://www.boeing.com/resources/boeingdotcom/commercial/about-our-market/assets/downloads/Boeing_Current_Market_Outlook_2015.pdf`, accessed 18-01-2018.

†Anonymous (IHS Markit), *"Bombardier CSeries,"* 2018. URL `https://janes.ihs.com/JAWADevelopmentProduction/Reference#`, accessed 15-03-2018.

Fig. 1 Wind tunnel model of an aircraft with tail-mounted propellers. Note: the wind tunnel results of this model are not studied in this paper. Photo credit: Nando van Arnhem

with tail-mounted propellers. In addition, a sensitivity analysis of each of the designs is carried out with respect to a subset of the assumptions that were made. The paper concludes with a summary of the main findings and an outlook to further research in this area in Section V.

II. Methodology

The main tool used for the research is the Aircraft Design Initiator, a conceptual, physics-based aircraft design tool created at Delft University of Technology. The goal of the Initiator is to combine empirical and inexpensive analysis methods with simple design rules to size aircraft based on a given set of top level requirements. In Figure 2 the design structure matrix of the tool is shown, demonstrating three, partially nested, design loops. The final design loop includes a physics-based weight estimation for the wing [12] and the fuselage [13]. The Initiator follows an iterative design approach where it converges to a feasible design, implying that all top-level requirements are satisfied and that the iterations converge to a constant maximum take-off weight.

The sizing of the horizontal tail plane is performed in conjunction with the longitudinal position of the wing using the X-plot (or scissor-plot) methodology. In the present paper, this procedure is performed neglecting the ground-effect and without applying wing positioning constraints stemming from the main landing-gear integration. The center-of-gravity bounds are determined by performing a loading analysis of passengers, luggage and fuel. The tail sizing process of the Initiator is described by Jansen and Vos[14] and has been extended with propeller installation effects. The resulting methodology uses stability and trim constraints in both power-off and power-on conditions as is shown in the flowchart of Figure 3. Power-on effects on the longitudinal stability and control include slipstream effects and propeller normal force. Research by Obert [6] showed the effect of the propeller slipstream on longitudinal stability and control for aircraft and presented the methods to predict their effect on lift and pitching moment coefficients. Vos and Bouquet connected this method to Drela's AVL Vortex Lattice Method[‡] and demonstrated that the slipstream effect on lift coefficient and pitching moment coefficient could be captured for wing-mounted propeller aircraft [7]. In the present methodology, the effect of the slipstream on the lift coefficient, lift-curve slope, and downwash gradient as described in [7] is used while the effect on the pitching moment about the center-of-gravity is included through a shift in the aerodynamic center as a result of the propeller slipstream and the flap deflection.

Although it is acknowledged that the tail should be sized for a long list of trim and stability requirements, including severe out-of trim effects, adequate control up to the dive Mach number, and sufficient damping of the short period motion, the present method limits the tail sizing to three requirements that are often sizing: static longitudinal stability

[‡]Drela, M., and Youngren, H., *"AVL (Athena Vortex Lattice),"* 2017. `http://web.mit.edu/drela/Public/web/avl/`

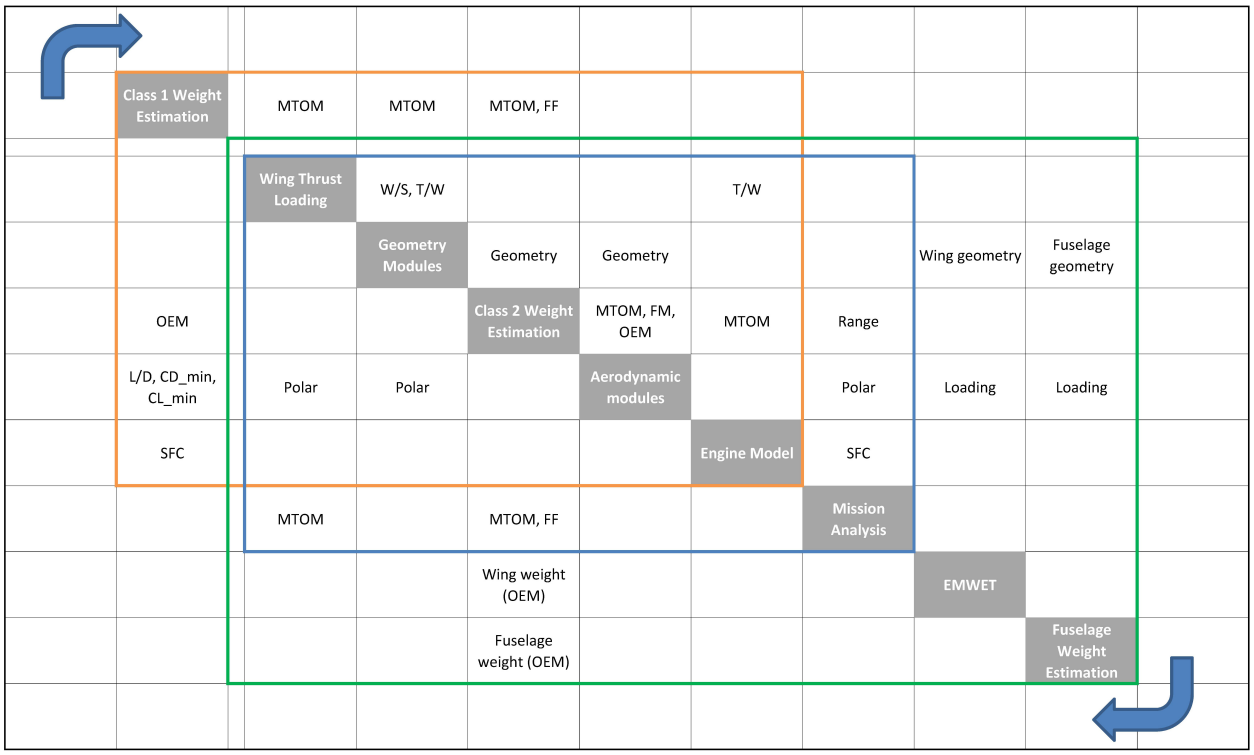

Fig. 2 Design Structure Matrix of the Initiator process flow. On the diagonal the main modules are shown, while on the off-diagonal cells the inputs/outputs of modules are displayed. The colored boxes indicate the three nested loops that the initiator executes iteratively.

in clean, take-off, and landing configuration, equilibrium up to the maximum lift coefficient in landing configuration, and take-off rotation in the take-off configuration at 1.2 times the stall speed. These result in 5 lines in the X-plot. As four of these requirements (excluding the take-off rotation) should be demonstrated in power-off and maximum power conditions, this results in a total of 9 constraint lines in the X-plot.

A. Stability

To compute the most aft position of the center of gravity for which static longitudinal stability is ensured, the following equation is employed:

$$\bar{x}_{\text{cg}} < \bar{x}_{\text{ac}_{\text{a-h}}} + \frac{C_{L_{\alpha_{\text{h}}}}}{C_{L_{\alpha}}}\left(1 - \frac{\text{d}\epsilon}{\text{d}\alpha}\right)\frac{S_{\text{h}}}{S}\frac{l_{\text{h}}}{\bar{c}}\left(\frac{V_{\text{h}}}{V}\right)^2 - \text{SM} \tag{1}$$

where $\bar{x}_{\text{cg}}$ is the center of gravity, $\bar{x}_{\text{ac}_{\text{a-h}}}$ is the aerodynamic center of the aircraft without the horizontal tail present, $C_{L_{\alpha_{\text{h}}}}$ is the lift-curve slope of the horizontal tail, $C_{L_{\alpha_{\text{a-h}}}}$ is the lift-curve slope of the aircraft-less tail, $\text{d}\epsilon/\text{d}\alpha$ is the downwash gradient, S_{h}/S the area ratio of the tail with respect to the wing, l_{h} is the distance between the quarter-chord points of the wing and the horizontal tail, $\bar{c}$ the mean aerodynamic chord, V_{h}/V is the velocity ratio at the horizontal tail plane with respect to the freestream velocity and SM is the longitudinal static margin, which is set by the designer. The tail-off lift-curve slope of the aircraft, the lift-curve slope of the horizontal tail plane, downwash gradient and the velocity ratio can all be affected by the propeller slipstream depending on the propeller position. Therefore, these are computed by numerically employing the method of Obert [6] in combination with AVL computations as described by Bouquet and Vos [7]. In power-off conditions, the velocity ratio for a t-tail is assumed to equal 1.0, while for a low-tail it assumed to be 0.85 due to its close proximity to the wing wake.

The location of the tail-off aerodynamic center ($\bar{x}_{\text{ac}_{\text{a-h}}}$) is computed as follows:

$$\bar{x}_{\text{ac}_{\text{a-h}}} = \bar{x}_{\text{ac}_{\text{w}}} + \frac{c_r d_{\text{f}}^2 FG}{\bar{c} C_{L_{\alpha_{\text{a-h}}}} S}\left[1 + 0.15\left(\frac{h_{\text{f}}}{d_{\text{f}}} - 1\right)\right] - (K_1 + \lambda K_2) + \sum k_{\text{n}} \frac{b_{\text{n}}^2 l_{\text{n}}}{S\bar{c} C_{L_{\alpha,\text{w+f}}}} - \begin{cases} 0.05 \sum \frac{B_{\text{p}} D_{\text{p}}^2 l_{\text{p}}}{S\bar{c} C_{L_{\alpha,\text{w+f}}}} & \text{if } C_T = 0 \\ 0 & \text{if } C_T \neq 0 \end{cases} \tag{2}$$

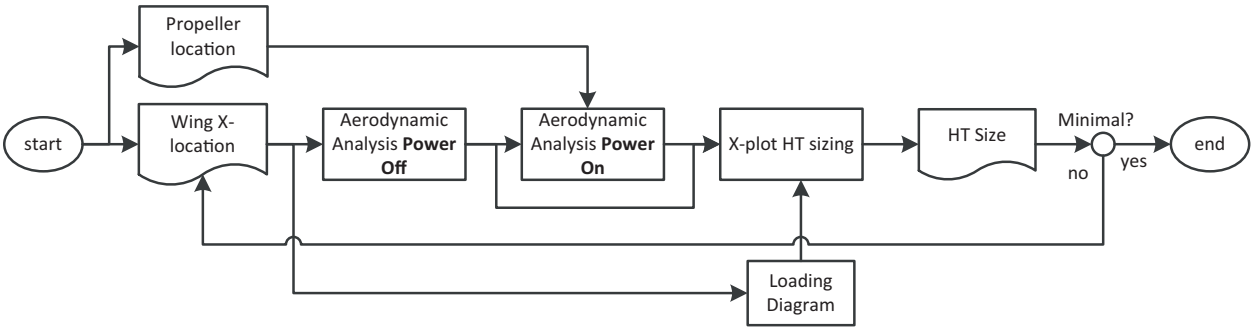

Fig. 3 Overview of horizontal tail (HT) sizing method.

The aerodynamic center of the wing ($\bar{x}_{\mathrm{ac_w}}$) is obtained from Torenbeek's Appendix E and is dependent on wing geometry and free-stream Mach number [15]. The second term and third term in Eq. 2 are due to the fuselage contribution and stem from ESDU [16]. It has been shown by Catalano that these corrections correlate well to wind tunnel results [17]. The equivalent wing root chord c_r, fuselage width d_f, fuselage height h_f and wing reference area S are all geometric properties of the aircraft. The constants F and K_1 are purely based on geometric properties and obtained from carpet plots. Similarly, constants G and K_2 scale with free stream Mach number (M_∞) only. The addition of the fuselage results in a forward shift of the aerodynamic center, although in power-on conditions this is somewhat damped due to the increase in lift gradient ($C_{L_{\alpha_{\mathrm{a\text{-}h}}}}$). The first summation term in Eq. 2 is due to the addition of engine nacelles, an empirical relation obtained from Torenbeek [15], where k_n is an empirical factor, b_n is the width of the nacelle, and l_n is length measured in negative x-direction between the wing's mean aerodynamic quarter chord point and the center of the nacelle. $C_{L_{\alpha,w+f}}$ is the lift-curve slope of the wing plus fuselage, which is dependent on power when the wing is in the slipstream of the propeller. The final summation term is due to windmilling propellers and scales with the number of blades (B_p), the square of the diameter of the propeller (D_p) and the distance (l_p) measured in negative x-direction between the propeller and the quarter-chord point on the mean aerodynamic wing chord. In case of power-on, this propeller effect on the aerodynamic center is absent and the effect of propeller thrust and normal force are included in other aerodynamic coefficients.

B. Equilibrium

Two cases of equilibrium are assessed: trim in flight and rotation about the main-landing gear axle. To trim the aircraft in flight, the following bound on the center of gravity is assumed:

$$\bar{x}_{\mathrm{cg}} > \bar{x}_{\mathrm{ac}} - \frac{C_{m_{\mathrm{ac}}}}{C_{L_{\mathrm{a\text{-}h}}}} + \frac{C_{L_\mathrm{h}}}{C_{L_{\mathrm{a\text{-}h}}}} \frac{S_\mathrm{h}}{S} \frac{l_\mathrm{h}}{\bar{c}} \left(\frac{V_\mathrm{h}}{V}\right)^2 \tag{3}$$

In the limit case, $C_{L_{\mathrm{a\text{-}h}}}$ equals the maximum tail-off lift coefficient of the aircraft, while C_{L_h} is the tail lift coefficient. This value is set to -0.8 [15] as the tail is unable to reach is maximum negative lift coefficient when exposed to a positive angle of attack. Together with the pitching moment coefficient, $C_{m_{\mathrm{ac}}}$ and the velocity ratio, these coefficients can all be influenced by the propeller slipstream depending on the relative location of the wing and tail plane with respect to the slipstream. Note that this also changes depending on the angle of attack. It should also be noted that both $C_{L_{\mathrm{a\text{-}h}}}$ and $C_{m_{\mathrm{ac}}}$ are a function of the flap setting. The most restraining condition is therefore with flaps deployed in landing configuration.

The aircraft-less-tail pitching moment about the aerodynamic center follows summation of contributing components:

$$C_{m_{\mathrm{ac}}} = C_{m_{\mathrm{ac,\,w}}} - 1.8\left(1 - \frac{2.5 d_\mathrm{f}}{l_\mathrm{f}}\right) \frac{\pi d_\mathrm{f} h_\mathrm{f} l_\mathrm{f}}{4 S \bar{c}} \frac{C_{L_0}}{C_{L_{\alpha,\mathrm{w+f}}}} + \Delta C_{m_{\mathrm{ac,\,HLD}}} + \begin{cases} -0.05 & \text{if } \bar{z}_\mathrm{n} > 0 \\ 0.02 & \text{if } \bar{z}_\mathrm{n} < 0 \end{cases} \tag{4}$$

where the starting point is the clean wing pitching moment $C_{m_{\mathrm{ac,\,w}}}$. This value is determined using the United States Air Force Data Compendium (USAF DATCOM).[18] The second contribution is due to the fuselage, where l_f is the fuselage length. The wing lift coefficient at zero angle of attack C_{L_0} is obtained from intersecting the lift curve obtained by AVL. This value is affected by flap deflection, the power setting and the wing-fuselage lift gradient $C_{L_{\alpha,\mathrm{w+f}}}$. The third contribution is due to the presence of High Lift Devices (HLD). This contribution is included for the take-off and

landing configuration and is determined for power-on and power-off conditions. The contribution is based on the method described by Torenbeek [15, App. G] and is dependent on the type of flaps, the flap chord ratio, the flap span ratio, and general wing parameters such as taper ratio, sweep angle and aspect ratio. The final component of Equation (4) accounts for the engine position and is a fixed value depending on $\bar{z}_{\text{n}}$, the vertical distance between the aircraft's center of gravity and the nacelles measured in positive z direction and normalized with the mean aerodynamic chord of the wing. In case the nacelle is below the aircraft $c.g.$ the contribution is nose-down and equal to -0.05. In case the nacelle is present above the $c.g.$ the pitching moment coefficient is increased by 0.02.

To rotate the aircraft during take-off, equilibrium around the main-landing-gear (mlg) wheel axle is assumed to find the most forward bound of the center-of-gravity [15]:

$$\bar{x}_{\text{cg}} > \bar{x}_{\text{mlg}} - \bar{z}_T \sum \frac{T}{W} - \left\{ \frac{C_{m_{\text{ac}}}}{C_{L_{\text{max}}}} - \eta_{\text{h}} \eta_q \frac{C_{L_{\text{h}}}}{C_{L_{\text{max}}}} \left[\frac{S_{\text{h}}}{S} \frac{l_{\text{h}}}{\bar{c}} - \frac{C_{L_{\text{R}}}}{C_{L_{\text{h}}}} (\bar{x}_{\text{cg}} - \bar{x}_{\text{ac}}) \right] \right\} \left(\frac{V_{\text{R}}}{V_{S_1}} \right)^2 \tag{5}$$

where $\bar{z}_T$ is the vertical distance between the aircraft's center of gravity and the thrust vector measured in positive z direction and normalized with the mean aerodynamic chord of the wing. The tail-off lift coefficient at rotation, $C_{L_{\text{R}}} = C_{L_0} + C_{L_{\alpha,\text{w+f}}} i_{\text{w}}$, with i_{w} being the wing incidence angle. Furthermore, V_{R}/V_{S_1} represents the margin between the stall speed in take-off configuration and the rotation speed (typically 1.05). Finally, η_h, accounts for the dynamic pressure over the tail surface according to:

$$\eta_{\text{h}} = \frac{\bar{x}_{\text{cg}} - \bar{x}_{\text{mlg}}}{l_{\text{h}}} \left(\frac{V_{\text{h}}}{V} \right)^2 \tag{6}$$

and η_q relates the tail lift capabilities for a given rate of rotation $\dot{\theta}_{\text{R}}$ as follows:

$$\eta_q = 1 + \frac{C_{L_{\alpha_{\text{h}}}}}{C_{L_{\text{h}}}} \frac{\dot{\theta}_{\text{R}} (\bar{x}_{\text{cg}} - \bar{x}_{\text{mlg}})}{V_{\text{R}}} \tag{7}$$

Again, it is emphasized that each of the aerodynamic coefficients and speeds appearing in the previous formulae can be influenced by the propeller slipstream depending on the inter-positioning of the propeller, wing and horizontal tail.

III. Verification & Validation

In this section two aircraft are automatically synthesized by means of the process documented in Section II. The resulting performance metrics, aircraft dimensions and characteristic weights are compared to values found in open literature. The goal of this section is to demonstrate that the aircraft design process results in conceptual aircraft designs that are relatively close to existing aircraft. This should give the reader confidence that this method is therefore capable to predict the impact of different propeller installation locations on the aforementioned performance metrics, which is presented in Section IV.

A. Aircraft Definition

The ATR-72 and Fokker 50 are chosen as reference aircraft to perform the validation study. The top-level aircraft requirements (TLARs) for these aircraft were derived from data that is available in the open literature[§¶] and is summarized in Table 1. While both aircraft are high-wing designs, the ATR-72 features a T-tail, while the Fokker 50 features a low tail. This is an important distinction as the horizontal tail plane of the ATR-72 is not in the slipstream of the propeller, while the tail of the Fokker 50 is. Furthermore, the ATR-72 retracts its main landing gear into the fuselage, while the Fokker 50 features a lengthened engine nacelle to retract the main landing gear into. As is apparent from Table 1, the ATR-72 carries more passengers than the Fokker 50 over a longer harmonic range, although the take-off distance of the Fokker 50 is appreciably shorter compared to the ATR-72.

B. Comparison Study

When using the TLARs from Table 1, the Initiator produces converged aircraft designs, which are shown in Figure 4. It can be seen that the geometry of the aircraft looks feasible. A more quantitative comparison on some of the overall vehicle characteristics is presented in Table 2. It can also be seen that the maximum take-off mass (MTOM) of both

[§] https://janes.ihs.com/JAWADevelopmentProduction

[¶] http://www.flyfokker.com

Table 1 TLARs for reference aircraft. Data from Jane's and Fokker documentation.

Spec.	Unit	ATR-72	F-50
Harmonic range	km	1530	1089
Structural payload	kg	7500	5500
Pax	-	68	50
Cruise altitude	m	7000	7620
Cruise Mach	-	0.45	0.46
Take-off distance	m	1333	891
Landing distance	m	915	1019

aircraft is within 5% of the reference values. This also holds for the operating empty mass (OEM) and the predicted shaft power.

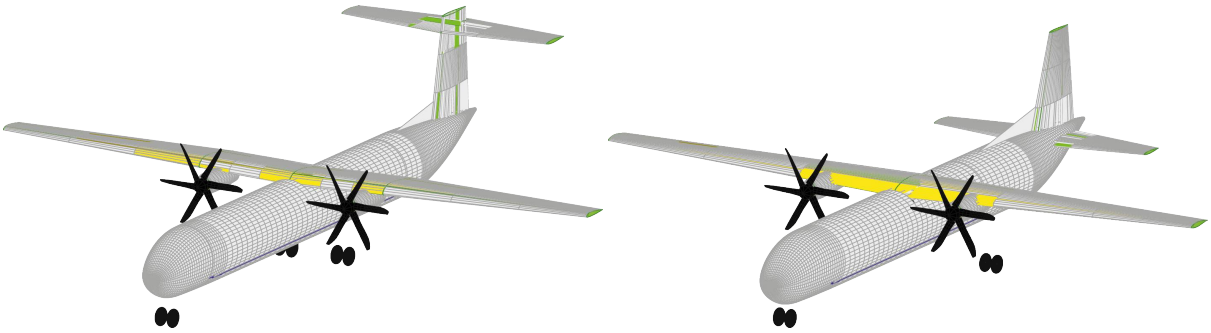

(a) ATR 72-600(I) (b) Fokker 50(I)

Fig. 4 Isometric view of aircraft designs produced by the Initator.

Table 2 also shows that the tail area is over-predicted for both aircraft. This could be due to 1) overestimation of the center of gravity excursion, 2) underestimation of any of the aerodynamic coefficients, or 3) incorrect design choices for tail positioning. The CG excursion of the Fokker 50 is estimated to be $0.25\overline{c}$, while for the ATR it is $0.29\overline{c}$ with the most forward CG located at $x/\overline{c} = 0.21$ and $x/\overline{c} = 0.18$, respectively.

In Figure 5 the scissor plots for both aircraft are displayed. The horizontal line indicates the bounds on the center-of-gravity (CG) excursion during loading. This has been obtained by evaluating the CG during loading of passengers, cargo and fuel. Each scissor plot shows six stability lines: three flap configurations times two power settings. In addition, there are three equilibrium lines, two in landing configuration (power on and power off) as well as one for take-off rotation (power on). First of all, it can be observed that the horizontal lines in either plot touch the most sizing equilibrium and stability bounds. This indicates that the wing is located in the longitudinal position where it results in the smallest tail area. For the ATR 72-600I, the horizontal tail area is sized by the power-off equilibrium in landing configuration and power-on stability in take-off configuration. For the Fokker 50I the tail is sized for power-off equilibrium in landing and power-off stability in take-off configuration. The difference between the sizing constraints is due to the location of the horizontal tailplane. For the Fokker 50 the tail is (partially) in the slipstream of the propeller, while for the ATR 72 it is not. This implies that the tail effectiveness of the Fokker 50 is much larger in power-on conditions. Therefore, the tail is merely sized for power-off conditions. For both aircraft, the propeller normal force and the propeller slipstream over the wing have a destabilizing effect on the aircraft. For the ATR 72-600I, this causes the power-on bounds to become sizing for the take-off condition.

The comparison study presented in this section shows that the proposed method for tail sizing is sensitive to the aerodynamic effects caused by the interference between the airframe and the propeller. However, it also shows that the tail size is overestimated by about 25% regardless of whether the tail is in the propeller slipstream or not. This implies that the results shown in the next section should be treated with some caution with respect to the absolute numbers that are being presented. The tail-off pitching moments and pitching-moment derivatives are evidently overestimated resulting in an over-conservative estimation of the tail size.

Table 2 Comparison of Initiator results to published data of the ATR 72-600 and Fokker 50. Data from Jane's

		ATR 72-600			Fokker 50		
	unit	Reference	Initiator	Difference	Reference	Initiator	Difference
MTOM	t	22.8	23.3	2%	20.8	20.2	-3%
OEM	t	13.3	13.5	2%	12.5	13.1	5%
P_{TO}	kW	3900	3590	-8%	3720	4140	11%
W_{TO}/P_{TO}	N/kW	57	64	12%	55	47.9	-13%
W_{TO}/S_w	N/m^2	3670	3330	-9%	2910	3010	3%
S_w	m^2	61	69	13%	70	66	-6%
b_w	m	27	28.7	6%	29	28.1	-3%
l_f	m	27	27.4	1%	25	25.8	2%
d_f	m	2.9	2.8	-2%	2.7	2.8	4%
d_p	m	3.9	4.0	3%	3.7	4.0	8%
S_h/S_w	(~)	0.19	0.24	27%	0.23	0.28	24%

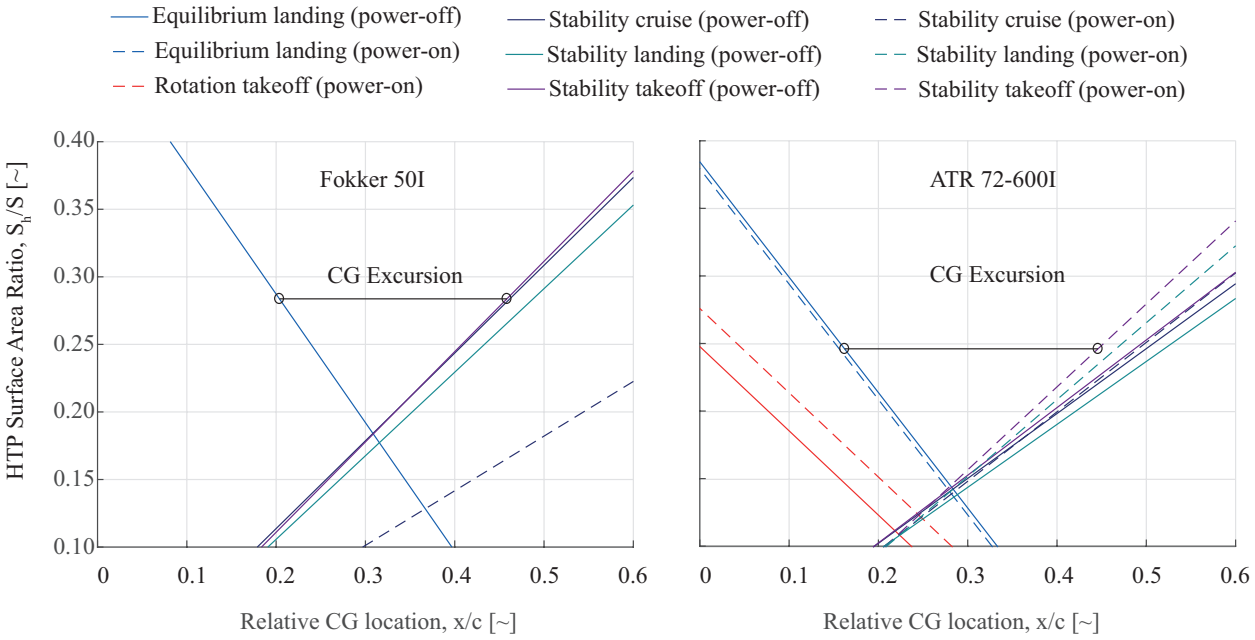

Fig. 5 Scissor plots created by the Initiator for the Fokker 50I (left) and the ATR 72-600I (right)

IV. Results

This section discusses the results of a comparison study between four regional turboprop (RTP) aircraft configurations. The overview of configurations is presented in Table 3. This set of designs is deemed to be representative in varying the position of the engines. Apart from the unconventional turboprop position aft of the fuselage and integrated in the stabilizer, the main wing engine designs feature an engine under a high wing and atop a low wing. The top-level aircraft requirements for the RTP under investigation in this paper are presented in Table 4. In the following subsections, first the top-level requirements and assumptions are presented and then the results of the synthesis are presented and discussed.

A. Synthesized Design Description

The converged design geometries of the four RTP aircraft are presented in Figure 6. The distinct engine and wing placement is visible for each aircraft. As can be seen, each aircraft has the same fuselage geometry. RTP3 and RTP4

Table 3 Layout configurations for new regional turboprop (RTP) aircraft

Name	Main wing	Engine	Hor. Stabilizer
RTP1	Low	Above wing	Conventional
RTP2	High	Below wing	T-Tail
RTP3	Low	Fuselage	T-Tail
RTP4	Low	Horizontal Tail	Conventional

Table 4 Top level requirements for conceptual RTP

Requirement	Value
max. passengers [-]	130
Payload mass [t]	13.6
harmonic range [km]	2960
M_{cruise} [-]	0.60
M_{tip} [-]	0.93
h_{cruise} [m]	8500
$l_{\text{take-off}}$ [m]	1350
l_{landing} [m]	1350
b_{max} [m]	36

Table 5 Input settings for conceptual RTP

Design	Value
seat pitch [m]	0.73
B_P [-]	10
$C_{L_{\text{max}}}$ (clean) [-]	1.6
$C_{L_{\text{max}}}$ (landing) [-]	3.0
δ_{HLD} (take-off) [°]	18
δ_{HLD} (landing) [°]	40
S.M. [% $\bar{c}$]	2%
BSFC [g/kW/h]	300

have their engines mounted further aft compared to RTP1 and RTP2. This results in a wing position which is mounted further aft on the fuselage as well as a larger horizontal tail plane. It can also be seen that the high-wing configuration yields the smallest horizontal tail plane (only 19% of the wing area), while RTP4 has a horizontal tail plane that has twice the area ratio (38% of wing area). Furthermore, one can see that for the low-wing configurations the proposed landing gear configuration would interfere with the flaps. This is due to the fact that the wing position is solely driven by the minimization of the horizontal tail surface area, and undercarriage integration constraints are not included.

To understand why the synthesized aircraft look so different, the stability and control properties are analyzed, starting with an analysis of the center-of-gravity (CG) excursion. The loading diagrams for each configuration, displaying all excursions, are depicted in Figure 7. From Figures 7(a) and 7(b) it can be seen that the wing-mounted configurations display a CG excursion of 25%$\bar{c}$ and 27%$\bar{c}$, respectively. The CG excursion for RTP3 and RTP4 is almost twice as large (see Figures 7(c) and 7(d)) and correspond to 55%$\bar{c}$ and 54%$\bar{c}$, respectively. As the mean aerodynamic chord ($\bar{c}$) of the latter two concepts is also larger, the absolute CG excursion for the two concepts with aft-mounted engines is more than double the absolute CG excursion of the wing-mounted configurations. These large excursions are a result of the placement of a relatively large mass (the turboprop engines) further aft on the fuselage in combination with the requirements of trimmability and stability for any combination of CG, flap deflection, and power setting.

The CG excursions are used to size the stabilizer, resulting in the scissor plots of Figure 8, where the black horizontal line represents the CG excursions. For all configurations, except RTP4, the aft CG limit is provided by the stability limit in power-on condition. Note that the stability lines all include a 2% static stability margine. For RTP1 this is the clean configuration whereas RTP2 and RTP3 are limited by stability in take-off configuration. These are limiting due to the absence of direct slipstream influence on the horizontal tail, resulting in the decrease of the ratio $C_{L_{\alpha_{\text{h}}}}/C_{L_{\alpha_{\text{a-h}}}}$. The lack of slipstream over the horizontal tail means the tail velocity ratio is below 1, reducing the effectiveness compared to the situation where the tail is (partially) immersed in the slipstream. Absence of the slipstream for RTP1 might seem unexpected as the tail configuration is conventional as opposed to the T-tail design of RTP2 and RTP3. However, the low wing mounted engines result in a slipstream deflected downward which does not intersect with the horizontal stabilizer. RTP2 benefits from the T-tail configuration, which reduces the effect of wing downwash gradient on the HTP, making it more effective as a stabilizing surface. As for RTP4, the most sizing condition occurs when the power is off due to the fact that the increase in dynamic pressure due to the propeller slipstream make the tail surface very effective as a stabilizer when the power is on. The lower the free stream velocity, the more the beneficial effects of this increased

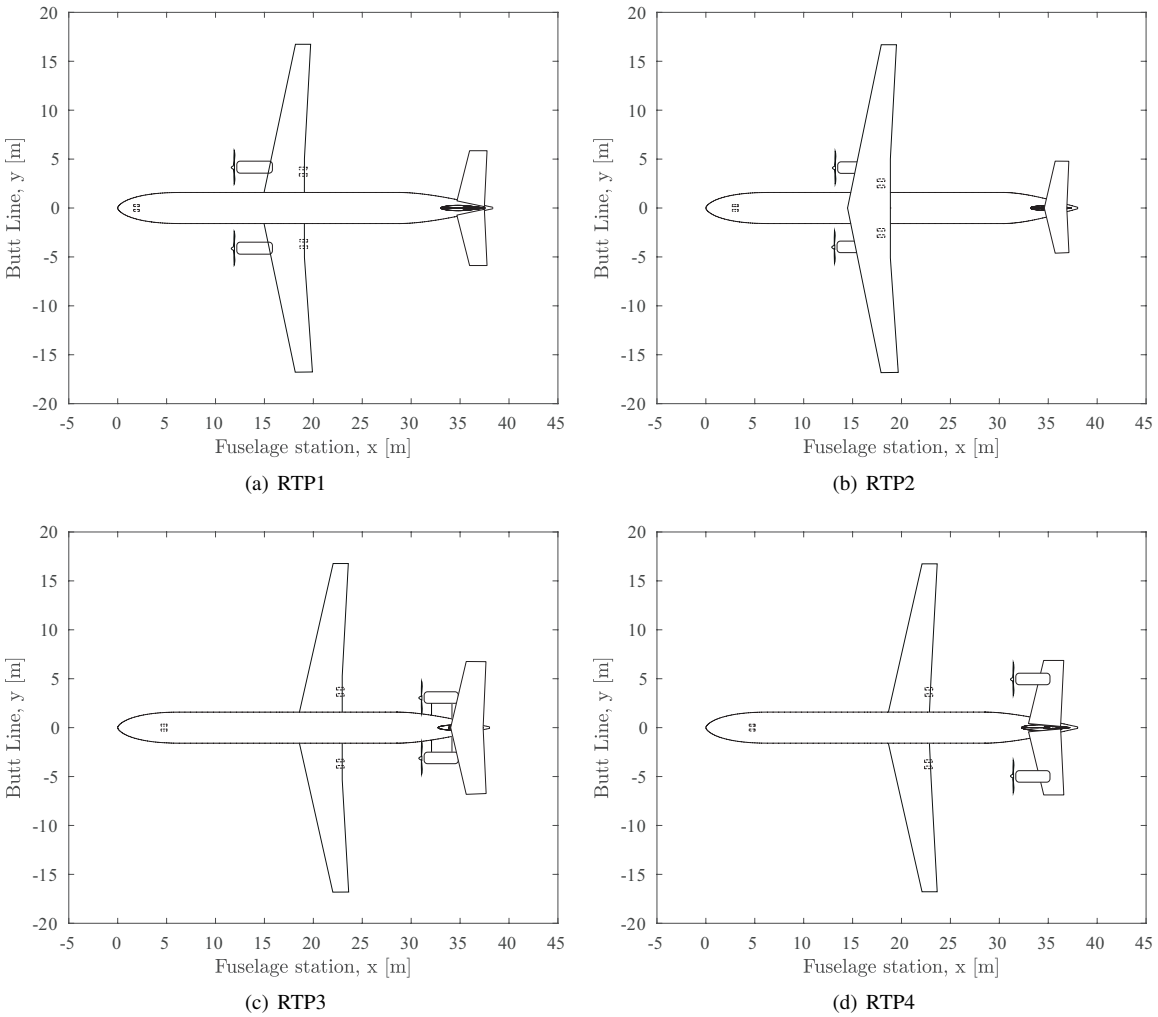

(a) RTP1 (b) RTP2

(c) RTP3 (d) RTP4

Fig. 6 Top view of RTP aircraft configurations

dynamic pressure are visible as shown by comparing cruise power-on stability to those depicting the same limit in take-off and landing. This is in line with the observations made for the Fokker 50(I) verification data of Figure 4(b).

Figures 8(a) and 8(b) show the configurations for which the forward CG is limited by the equilibrium in landing configuration. These limits are defined by the strong nose-down pitching moment of the configuration stemming from the deployment of the high-lift devices. The effect of power is minimal due to the engine vertical position aligning the thrust vector with the vertical $c.g.$ position, preventing the thrust from adding to the pitching moment coefficient. As the slipstream effect on pitching moment is not included in the methodology, the difference between powered and upowerd condition on the tail-off pitching moment is small. For RTP3 in Figure 8(c) the most forward CG is limited by the take-off rotation requirement. This results from the required aft placement of the main wing in order to compensate for the engine placement at the rear of the aircraft. The main landing gear position is tied to the main wing position, meaning this system is also positioned further aft. As a result, the targeted rotational rate of $\dot{\theta} = 0.052\ {}^{\text{deg}}/_{\text{s}^2}$ about this main gear position is more limiting than the trim in landing configuration. The difference between RTP3 and RTP4 for this rotation limit is the power setting. For RTP3 the stabilizer is outside the slipstream in take-off configuration, while for RTP4, the tail is immersed in the slipstream of the propeller. Therefore, the tail is very effective in providing forces or force-derivatives. In case of the take-off, the constraining line to achieve equilibrium allows such a large forward center of gravity, that it falls outside the bounds of Figure 8(d). Due to the improved effectiveness of the tail in power-on conditions, the sizing requirement is indeed the power-off requirement of achieving the maximum lift coefficient in landing configuration.

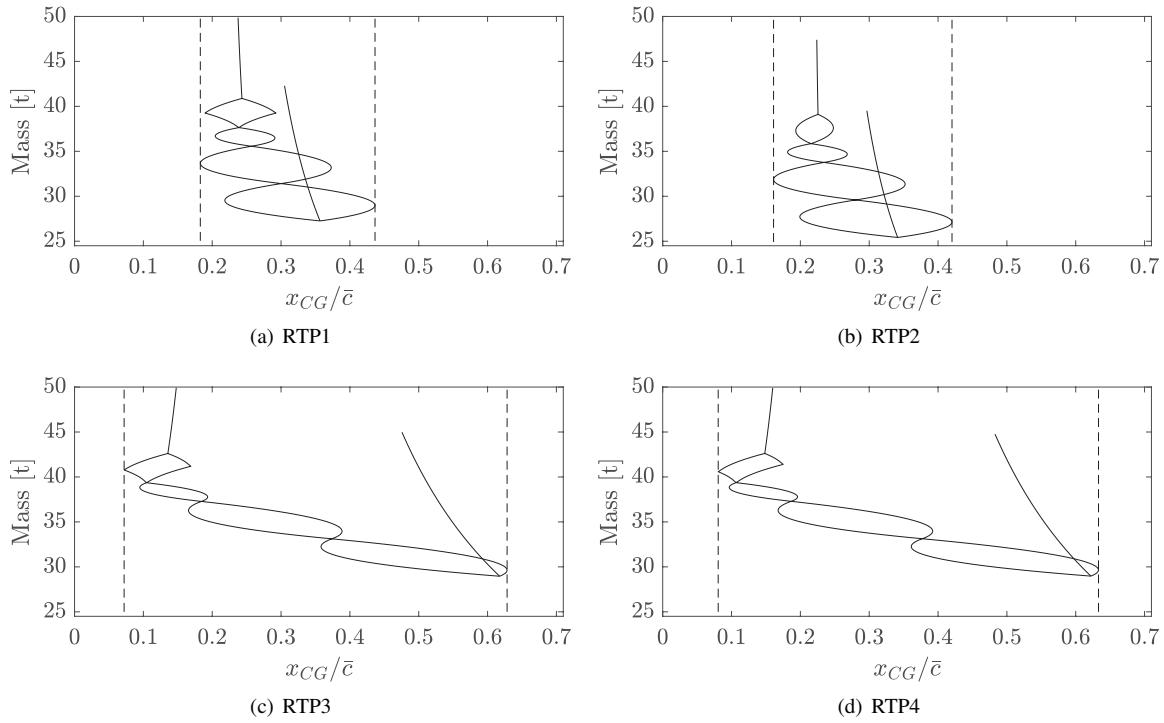

(a) RTP1 (b) RTP2

(c) RTP3 (d) RTP4

Fig. 7 Loading diagrams showing forward and aft center-of-gravity (CG) limits as fraction of mean aerodynamic chord ($\bar{c}$)

.

The black horizontal lines in the graphs of Figure 8 show the center-of-gravity excursion that is present during loading. Their vertical location in the plot indicates the required tail area ratio that is required to fulfill the sizing requirements in terms of equilibrium and stability. While the two engine-mounted configurations have a relatively small tail ratio, 27% and 19% respectively, the tail ratio for the two aft-mounted propellers is significantly higher, 36% and 38% respectively. This results in considerably larger horizontal tail planes for the latter two configurations (RTP3 and RTP4), which results in more weight and more friction drag.

B. Key Performance Indicators

The RTP performance is captured in a set of Key Performance Indicators (KPIs) which are presented for the four RTP aircraft in Table 6: maximum take-off mas s(MTOM), operating empty mass (OEM), fuel burn per passenger per 100 kilometers over the harmonic mission range (without diversion), the tail area ratio, the parasite drag area ($C_{D_0} \times S$w) and the trim drag at start of cruise.

Table 6 Key performance indicators for converged Initiator RTP configurations. Note: the trim drag coefficient is computed at the start of the cruise phase for the harmonic mission.

Aircraft	MTOM [t]	OEM [t]	FM [t]	fuel [l/pax/100km]	S_h/S_w [-]	Par. Drag Area [m^2]	$C_{D_{trim}}$ * [cts]
RTP1	50	27	9.0	2.6	0.27	2.2	8
RTP2	47	25	8.3	2.4	0.19	2.1	8
RTP3	52	29	9.5	2.8	0.36	2.4	26
RTP4	52	29	9.5	2.8	0.38	2.4	20

*forward $c.g.$ position, start of cruise

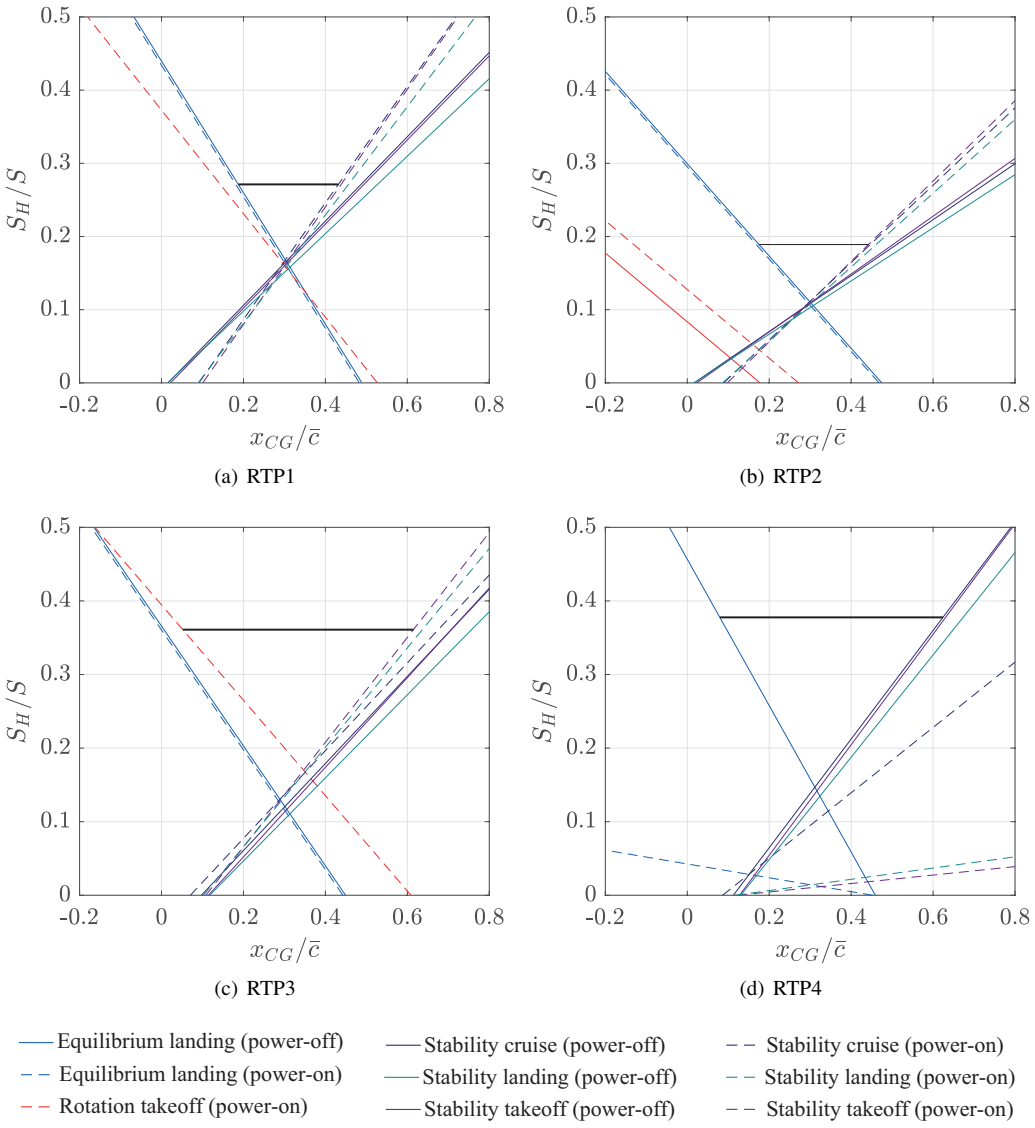

Fig. 8 Scissor plots showing horizontal stabilizer area ratio for CG excursion of Figure 7

In this comparison, RTP2, the high-wing aircraft with wing-mounted engines and a T-tail, comes out as the best aircraft in terms of maximum take-off mass and the the required fuel mass. It is also the aircraft with by far the smallest horizontal tail plane, which has the same ratio as the ATR 72-600 (see Table 2). RTP1 also performs rather well, although it has a larger tail area and burns about 5% more fuel over the design mission compared to RTP2. Note that the trim drag that is quoted for most forward CG position is rather the same for both aircraft. In practice, the CG is likely to be located somewhat further aft, reducing the trim drag penalty. Parasite drag area of the two aircraft is also within 5% difference.

RTP3 and RTP4 show a distinct deterioration in key performance indicators. The take-off mass increases to 52 tonnes, more than 10% higher than RTP2. This increase is attributed to the larger tail area, stemming from the increase in tail area ratio, a large trim drag penalty, and an increased wing mass due to the absence of the bending-moment relief of the wing-mounted engines. While the trim drag penalty that is quoted in the last column of Table 6 is representative of a worst-case scenario, it is likely not to be far off if the loading diagrams of Figure 7(c) and Figure 7(d) are examined. They show that for a fully packed aircraft, the CG is quite close to the most forward bound and the shift due to fuel burn is very small. Therefore, the trim drag penalty persists throughout the entire flight, which has a detrimental effect on the

required fuel mass. If the trim drag penalty could be relieved by, for example, adding a trim tank in the tail, roughly 5% of total drag in cruise conditions could be reduced which would already bring the fuel burn of these aft-mounted propeller aircraft closer to the wing-mounted propeller aircraft.

The 15% increase in parasite drag area of RTP3 and RTP4 compared to RTP2 cannot simply be solved by adding a trim tank in the tail. This increase is largely due to the increase in tail size as well as the larger wing area. If one wishes to reduce this penalty, the CG excursion should be limited such that the wing can shift further forward without making the aircraft statically unstable when the aircraft is empty. A more forward position of the wing would imply that the tail download during cruise can be reduced and the trim drag penalty can be thus be lowered. To ensure that with a more forward location of the wing the aircraft is still statically stable when empty, a water ballast tank could be added in the nose cone of the fuselage. Such a tank would only be filled with water ballast when the aircraft would fly without passengers (i.e. ferry flights). Water ballast tanks have been successfully used to limit the CG excursion on aircraft with fuselage-mounted turbofan engines such as the Ilyushin 62, the Tupolev 154 and the Sud Aviation SE 210 Caravelle.

V. Conclusion

Four different propeller-powered aircraft configurations designed for a mission to carry 130 passengers over a harmonic range 2960km have been conceived using an automated aircraft synthesis method. It was shown that the tail sizing method, which includes the effect of the propeller normal force as well as the slipstream effect on wing and tail lift, is sensitive to center-of-gravity excursion, propulsive power, and flap deflection, yet over predicts the horizontal tail area by about 25%, when compared to reference aircraft. Of the four configurations that were assessed using this method, the high-wing aircraft with wing-mounted propellers had the lowest take-off mass (47t), lowest fuel burn (2.4 l/pax/100km) and the smallest tail area (19% of the wing area). A configuration with pylon-mounted propellers mounted aft on the fuselage and a configuration with tail-mounted propellers showed a 10% increase in maximum take-off mass and a 15% increase in fuel consumption, compared to their wing-mounted counterpart. These increases were attributed to the much larger horizontal tail size (36% and 38% of wing area, respectively) and a large trim drag penalty. These, in turn, were caused by the large center-of-gravity excursion resulting from the aft location of the engines. Proposed modifications to these configurations to reduce this excursion include the addition of a trim tank in the tail to reduce trim drag during cruise or a water ballast tank in combination with a more forward position of the wing. Further studies are required to demonstrate their effect.

References

[1] Babikian, R., Lukachko, S. P., and Waitz, I. A., "The historical fuel efficiency characteristics of regional aircraft from technological, operational, and cost perspectives," *Journal of Air Transport Management*, Vol. 8, No. 6, 2002, pp. 389–400. doi:10.1016/S0969-6997(02)00020-0.

[2] Nicolosi, F., Corcione, S., Trifari, V., Cusati, V., Ruocco, M., and Della Vecchia, P., "Performance Evaluation and DOC Estimation of an Innovative Turboprop Configuration," *Proceedings of the 2018 Aviation Technology, Integration, and Operations Conference*, Atlanta, GA, 2018.

[3] Goldsmith, I. M., "A study to define the research and technology requirements for advanced turbo/propfan transport aircraft," Technical report, McDonnell Douglas Corporation, 1981.

[4] Vos, R., and Hoogreef, M. F. M., "System-Level Assessment of Tail-Mounted Propellers for Regional Aircraft," *Proceedings of the 31st Congress of the International Council of Aeronautical Sciences*, Belo Horizonte, Brazil, 2018.

[5] Veldhuis, L. L. M., "Review of Propeller-Wing Aerodynamic Interference," *Proceedings of the 24th Congress of the International Council of Aeronautical Sciences*, 2004.

[6] Obert, E., "The Effect of Propeller Slipstream on the Static Longitudinal Stability and Control of Multi-Engined Propeller Aircraft," *Proceedings of the 19th Congress of the International Council of Aeronautical Sciences*, 1994.

[7] Bouquet, T., and Vos, R., "Modeling the propeller Slipstream Effect on Lift and Pitching moment," *Proceedings of the 2017 AIAA Aerospace Sciences Meeting*, Grapevine ,TX, 2017, pp. 1–15. doi:10.2514/6.2017-0236.

[8] Arnhem, N. v., Sinnige, T., Stokkermans, T. C., Eitelberg, G., and Veldhuis, L. L. M., "Aerodynamic Interaction Effects of Tip-Mounted Propellers Installed on the Horizontal Tailplane," *2018 AIAA Aerospace Sciences Meeting*, Orlando, Fl, 2018. doi:10.2514/6.2018-2052.

[9] Elmendorp, R., Vos, R., and La Rocca, G., "A Conceptual Design and Analysis Method for Conventional and Unconventional Airplanes," *Proceedings of the 29th Congress of the International Council of Aeronautical Sciences*, St. Petersburg, Russia, 2014.

[10] Brown, M., and Vos, R., "Conceptual Design and Evaluation of Blended-Wing Body Aircraft," *Proceedings of the 2018 AIAA Aerospace Sciences Meeting*, American Institute of Aeronautics and Astronautics, 2018. doi:10.2514/6.2018-0522.

[11] Vos, R., Wortmann, A., and Elmendorp, R., "The optimal cruise altitude of LNG-fuelled turbofan aircraft," *Journal of Aerospace Operations*, Vol. 4, No. 4, 2017, pp. 207–222. doi:10.3233/AOP-160063.

[12] Elham, A., La Rocca, G., and Vos, R., "Refined Preliminary Weight Estimation Tool for Airplane Wing and Tail," *Aerospace Technology Conference and Exposition, SAE Technical Paper 2011-01-2765*, 2012, p. 11. doi:10.4271/2011-01-2765.

[13] Schmidt, K., and Vos, R., "A Semi-Analytical Weight Estimation Method for Oval Fuselages in Conventional and Novel Aircraft," *Proceedings of the 52nd AIAA Aerospace Sciences Meeting*, 2014. doi:10.2514/6.2014-0026.

[14] Jansen, W., and Vos, R., "Asessing the Effect of Decreased Longitudinal Stability on Aircraft Size and Performance," *Proceedings of the 54th AIAA Aerospace Sciences Meeting*, 2016. doi:10.2514/6.2016-1281.

[15] Torenbeek, E., *Synthesis of Subsonic Airplane Design*, Delft University Press, 1976.

[16] Anonymous, "Aerodynamic centre of wing-fuselage combinations," Data item 76015, Engineering Sciences Data Unit (ESDU), 1976.

[17] Catalano, F., and Costanzo, F., "Theoretical and experimental analysis of the fuselage influence on the wing aerodynamic center position at low speed conditions," *22nd International Congress of Mechanical Engineering*, ABCM, Ribeirão Preto, Brazil, 2013, pp. 2089–2100.

[18] Finck, R., "USAF (United States Air Force) Stability and Control DATCOM (Data Compendium)," Technical report, McDonnell Aircraft Co., St. Louis, 1978.